

Article

Morphology Control of $\text{PbZr}_x\text{Ti}_{1-x}\text{O}_3$ Crystallites under Alkaline Hydrothermal Conditions

Marjeta Maček Kržmanc ^{1,*}, Zdravko Kutnjak ² and Matjaž Spreitzer ¹¹ Advanced Materials Department, Jožef Stefan Institute, Jamova 39, 1000 Ljubljana, Slovenia² Department of Condensed Matter Physics, Jožef Stefan Institute, Jamova 39, 1000 Ljubljana, Slovenia

* Correspondence: marjeta.macek@ijs.si

Abstract: Outstanding ferroelectric and piezoelectric properties of $\text{PbZr}_x\text{Ti}_{1-x}\text{O}_3$ (PZT) make nano and sub-micrometer particles of this material interesting for future nanotechnological applications as well as for fundamental studies of ferroelectricity at the nanoscale. In the present work, the prospects of a new hydrothermal approach were explored to control the particle size, aggregation stage, and composition of the PZT with the target composition of $\text{Zr}/\text{Ti} = 60/40$ ($x = 0.6$). Starting with water-soluble Zr-, Ti-, and Pb-precursors, the PZT formation was examined in the broad base (KOH) concentration range. The PZT particle size and composition were governed by the ratio of KOH with respect to Pb and not by the absolute KOH concentration (c_{KOH}). The incorporation of Zr into the PZT perovskite phase began to decline at $\text{KOH}:\text{Pb} \leq 1.7$ and at $\text{KOH}:\text{Pb} > 20$. In the concentration range of $20 \geq \text{KOH}:\text{Pb} > 1.5$, the PZT particles adopted a cube-like shape, the size of which decreased with a decrease in the $\text{KOH}:\text{Pb}$ ratio. The smallest (< 200 nm) and well-separated PZT particles were obtained at $\text{KOH}:\text{Pb} = 1.7$. The prevailing PZT crystal structure at a Zr/Ti composition of around 60/40 was rhombohedral; the tetragonal phase also began to appear in Ti-richer PZT compositions ($\text{Zr}/\text{Ti} \leq 50/50$). The developed understanding established the basis for further tailoring of PZT particle morphologies for application-oriented or fundamental research.

Keywords: $\text{PbZr}_x\text{Ti}_{1-x}\text{O}_3$; hydrothermal synthesis; ferroelectric particles; perovskites



Citation: Kržmanc, M.M.; Kutnjak, Z.; Spreitzer, M. Morphology Control of $\text{PbZr}_x\text{Ti}_{1-x}\text{O}_3$ Crystallites under Alkaline Hydrothermal Conditions. *Crystals* **2022**, *12*, 1514. <https://doi.org/10.3390/cryst12111514>

Academic Editors: Alexander Martin and Hana Uršič

Received: 28 September 2022

Accepted: 19 October 2022

Published: 25 October 2022

Publisher's Note: MDPI stays neutral with regard to jurisdictional claims in published maps and institutional affiliations.



Copyright: © 2022 by the authors. Licensee MDPI, Basel, Switzerland. This article is an open access article distributed under the terms and conditions of the Creative Commons Attribution (CC BY) license (<https://creativecommons.org/licenses/by/4.0/>).

1. Introduction

Exceptional dielectric, ferroelectric, pyroelectric, and piezoelectric properties of $\text{PbZr}_x\text{Ti}_{1-x}\text{O}_3$ (PZT) have already been exploited in many practical devices such as piezoelectric transducers, microelectromechanical systems (MEMS), pyroelectric infrared detectors, and many others [1–4]. Due to such great application potential, PZT has been prepared and studied as thin films [5], sintered ceramics [6], single crystals [7], and free-standing nanoparticles [8]. PZT compositions with Zr content in the range of $0.4 < x < 0.6$ have aroused the greatest scientific curiosity due to the best ferroelectric and piezoelectric properties around the morphotropic phase boundary (MPB) ($\text{Zr}/\text{Ti} = 52/48$ ($x = 0.52$)). Bulk PZT with $0 \leq x \leq 0.52$ and with $0.52 < x \leq 1$ exhibit a tetragonal (P4mm) and rhombohedral (R3c) crystal structure, respectively [1]. PZT nano and sub-micrometer particles are foreseen for many advanced future applications in printed electronics, composites for sensors and actuators, 3D printing [4], and piezoelectric energy harvesting devices [9]. Moreover, PZT nanoparticles are also of great interest in the fundamental studies of ferroelectricity at the nanoscale and experimental demonstrations of the Hopfion and vortex topological states in ferroelectric nanoparticles [10]. Since the development of lead-free piezoelectrics has not yet reached the stage to fulfill all application-related properties (costs, mechanical and thermal properties, reproducibility, electrical conductivity, and lifetime), PZT is still allowed to be used in piezoelectric devices despite toxic environmental issues that arise from evaporation of Pb at high calcination and sintering temperatures [11,12]. Furthermore, PZT ceramics and nanoparticles also attract great scientific attention in obtaining a

general understanding of the origin of high piezoelectricity at the MPB and ferroelectricity at the nanoscale, respectively. These are the main reasons why PZT is still the subject of scientific research.

Many of above-mentioned nanotechnology applications require non-aggregated particles with a narrow size distribution and well-defined composition. The hydrothermal method has been proved as one of the most appropriate methods for preparation of various controlled morphologies of perovskites [13–18], including synthesis of PZT solid solutions.

Despite quite a few reports that dealt with the formation of PZT under hydrothermal or solvothermal conditions [2–4,8,19–21], systematic conclusions about the effect of a particular experimental parameter on the PZT morphology were difficult to infer from these studies. The determinations of systematic correlations were hindered because the syntheses were performed using various Zr- and Ti-precursors (TiCl_4 and ZrCl_4 [21], alkoxides [20], Ti-alkoxides and water-soluble Zr-precursor [3,8,19], etc.). In these studies, precipitation and alkali conditions in hydrothermal media were exclusively achieved by a KOH mineralizer, the concentration of which was typically expressed in mol/L without the indication of the concentration correlations between KOH and perovskite ions (Pb^{2+} , Zr^{4+} , Ti^{4+}). The morphological development of PZT in a wide KOH concentration range is also yet to be systematically addressed. In the present work, we attempted to fill above-mentioned knowledge gaps in the understanding of key principles that govern the morphological development of PZT under hydrothermal conditions. In this study, the proposed hydrothermal synthesis route for formation of PZT from water-soluble $\text{ZrOCl}_2 \cdot 8\text{H}_2\text{O}$ and titanium(IV) bis(ammonium lactato) dihydroxide (TALH) was new and simple. The latter stemmed from the fact that no organic solvents or stabilizers were needed for preparation of the homogeneous solution of both precursors or to control their hydrolysis rates, respectively. The main goal of the work was to examine the formation of PZT in a broad KOH concentration range and to determine the optimal base concentration for formation of non-aggregated sub-100 nm PZT particles with the target PZT composition of $\text{Zr}/\text{Ti} = 60/40$. In the future, we would like to experimentally confirm the existence of hopfions in such particles as was predicted by Luk'yanchuk et al. [10]. The concentration of the KOH solution was expressed with respect to perovskite ions (specifically $\text{KOH}:\text{Pb}$) and we proved that this parameter determined the PZT morphology and not the absolute KOH concentration.

The presented systematic research identified the experimental conditions for formation of non-aggregated PZT particles with sub-200 nm particle size and composition close to MPB. Developed understanding establishes the basis for further optimization of the size and composition of the PZT particles, that can find several interesting applications and serve as model system for fundamental studies of nanoscale ferroelectricity.

2. Materials and Methods

2.1. Chemicals

The chemicals used for the syntheses of PZT crystallites were: a titanium(IV) bis(ammonium lactato) dihydroxide (TALH) water solution with a thermogravimetrically determined 55.2 wt % of the TALH precursor (Aldrich, St. Louis, MO, USA); zirconyl chloride octahydrate ($\text{ZrOCl}_2 \cdot 8\text{H}_2\text{O}$, 98% (Acrocs Organics, Geel, Belgium); lead (II) acetate trihydrate ($\text{Pb}(\text{OOCCH}_3)_2 \cdot 3\text{H}_2\text{O}$, 99% (Alfa Aesar, Haverhill, MA, USA); and potassium hydroxide (KOH, $\geq 85\%$ (Sigma-Aldrich)). Syntheses were performed using ultra-pure water (18.2 M Ω .cm; Purelab Option-Q7, ELGA).

2.2. Synthesis Procedure

The preparation of the $\text{PbZr}_x\text{Ti}_{1-x}\text{O}_3$ (PZT) crystallites with the target compositions corresponding to $x = 0.6$ (PZT06, $\text{Zr}/\text{Ti} = 60/40$), $x = 0.7$ (PZT07, $\text{Zr}/\text{Ti} = 70/30$), and $x = 0.8$ (PZT08, $\text{Zr}/\text{Ti} = 80/20$) included three major steps: (i) precipitation of initial precursors, (ii) a hydrothermal reaction, and (iii) washing of the reaction product and removal of the excessive amount of $\text{PbO} \cdot \text{H}_2\text{O}$ with 1 M of HNO_3 . In all syntheses, $\text{Pb}(\text{OOCCH}_3)_2 \cdot 3\text{H}_2\text{O}$ was applied in excess of 25% with respect to the titanium and zirconium precursors (molar ratio:

$\text{Pb}/(\text{Zr} + \text{Ti}) = 1.25$). The amounts of added KOH are expressed as KOH:Pb molar ratios; for easier comparison with the literature data, the content of KOH is also given in mol/L (Table 1). For the target composition of $x = 0.6$, the initial precursors were precipitated either in one step or in two steps (with intermediate precipitation of a Ti-Zr gel). In the one-step synthesis procedure, the individual precursors were dissolved in ultra-pure water in amounts resulting in the initial concentrations presented in Table 1. The starting solutions of TALH, ZrOCl_2 , and KOH were prepared in glass beakers while the $\text{Pb}(\text{OOCCH}_3)_2 \cdot 3\text{H}_2\text{O}$ was dissolved directly in the Teflon (PTFE) insert of a Parr autoclave. For the preparation of the homogeneous solution of TALH and ZrOCl_2 , appropriate volumes of both solutions were mixed together to provide the initial target Zr/Ti ratio. The precipitation started with the addition of the KOH solution to a water solution of lead acetate; finally, the solution of the mixed Ti-Zr precursor was also added dropwise to this alkaline suspension of white precipitate in the PTFE insert. All of the Pb-, Ti-, and Zr-precursors precipitated under these alkaline conditions. A PTFE insert containing 50 mL of alkaline suspension was closed in a stainless steel Parr autoclave (4748) that was put in preheated oven at 235 °C and kept at this temperature for 12 h and then cooled down to room temperature by natural cooling. The one-step precipitation procedure was applied for PZT at $x = 0.6$ and higher KOH:Pb molar ratios ($3 \leq \text{KOH:Pb} \leq 40$). To enable formation of a pure perovskite phase at $\text{KOH:Pb} < 4$, the Zr- and Ti-precursors were precipitated separately and the formed Ti-Zr gel was washed until reaching a neutral pH and added to the precipitated $\text{PbO} \cdot \text{H}_2\text{O}$ before a hydrothermal reaction, which also took place at 235 °C for 12 h. This so-called two-step precipitation process was applied in the synthesis of PZT at the proposed $x = 0.6$, $x = 0.7$, and $x = 0.8$ and $1.5 \leq \text{KOH:Pb} \leq 3$. In all cases, the intermediate precipitation of the Zr-Ti-precursors was conducted with an excessive amount of KOH corresponding to $(\text{KOH}/(\text{Zr} + \text{Ti})) = 7.8$. The concentrations of the Pb^{2+} , Zr^{4+} , and Ti^{4+} ions that were bound in various precipitates in the precursor solutions before the hydrothermal reaction are presented in Table 1. After the hydrothermal treatment, the reaction product was firstly washed with water to remove excess alkalis and other dissolved ions. In next step, the precipitate was soaked in 1 M of HNO_3 for 5 min. This short-time acid treatment did not influence the perovskite PZT phase but dissolved the excessive $\text{PbO} \cdot \text{H}_2\text{O}$. Then, the remains of acids were eliminated using water washing. Finally, the powder was washed with ethanol and dried in ambient conditions.

2.3. Characterization

The phase composition and crystal structure of the synthesized PZT samples were investigated via powder X-ray diffraction (XRD) measurements using a PANalytical X'Pert PRO MPD X-ray diffractometer (Almelo, the Netherlands) with $\text{CuK}\alpha_1$ radiation ($\lambda = 1.5406 \text{ \AA}$). The XRD patterns were collected in the range of 20° to 70° 2θ in steps of 0.026° with an integration time of 500 s. The morphology and chemical compositions of the as-prepared PZT particles were examined using field-emission scanning electron microscopes (FE-SEM; JEOL JSM-7600 F and Thermo Fischer Verios 4G HP, Waltham, MA, USA) equipped with an Oxford Instruments energy-dispersive X-ray spectrometer (EDS). The particle sizes (the lengths of the cube edges) were evaluated in the SEM images with the help of Smile View software (JEOL, Tokyo, Japan). For the statistics, at least 200–300 particles were assessed to determine the average lengths of the cube edges. Elemental and chemical compositions of the PZT particles were determined with an Oxford EDS system (Ultim Max SDD 65 mm²) attached to the Thermo Fisher Verios 4G HP. PZT particles were coated with carbon (6 nm) to prevent charging and at least 7 particles of each type of the PZT sample were analyzed and the average compositions were calculated.

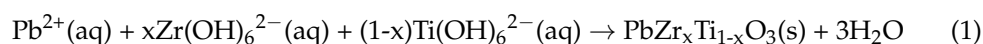
Table 1. Synthesis details in preparation of $\text{PbZr}_x\text{Ti}_{1-x}\text{O}_3$ (PZT) crystallites with the target $x = 0.6$ (PZT06), $x = 0.7$ (PZT07), and $x = 0.8$ (PZT08) compositions: concentrations of initial solutions before mixing together and concentrations in the autoclave before hydrothermal reactions.

Target Composition (Synthesis Approach)	Concentrations (mol/L)																
	Concentrations of Initial Solutions (mol/L)							Concentrations in the PTFE Insert before Hydrothermal Reaction (mol/L)									
PZT06 (one-step)	TALH *							0.112									
	ZrOCl ₂ ·8H ₂ O							0.168									
	Pb(OOCCH ₃) ₂ ·3H ₂ O							0.175									
	KOH (OH:Pb)	40:1	30:1	20:1	6:1	5:1	4:1	3:1	40:1	30:1	20:1	6:1	5:1	4:1	3:1		
	KOH (mol/L)	3.5	2.6	1.75	0.53	0.44	0.35	0.26	1.400	1.050	0.700	0.210	0.175	0.140	0.110		
PZT06 (two-step)	TALH *							0.112									
	ZrOCl ₂ ·8H ₂ O							0.14									
	Pb(OOCCH ₃) ₂ ·3H ₂ O							0.175									
	KOH (OH:Pb)	3:1		2:1		1.7:1		1.5:1		3:1		2:1		1.7:1		1.5:1	
	KOH (mol/L)	0.750		0.500		0.429		0.735		0.1050		0.070		0.0600		0.053	
PZT07 (two-step)	TALH *							0.084									
	ZrOCl ₂ ·8H ₂ O							0.163									
	Pb(OOCCH ₃) ₂ ·3H ₂ O							0.175									
	KOH (OH:Pb)	3:1		2:1		1.7:1		1.5:1		3:1		2:1		1.7:1		1.5:1	
	KOH (mol/L)	0.750		0.500		0.429		0.735		0.105		0.070		0.060		0.053	
PZT08 (two-step)	TALH *							0.056									
	ZrOCl ₂ ·8H ₂ O							0.187									
	Pb(OOCCH ₃) ₂ ·3H ₂ O							0.175									
	KOH (OH:Pb)	3:1		2:1		1.7:1		1.5:1		3:1		2:1		1.7:1		1.5:1	
	KOH (mol/L)	0.750		0.500		0.429		0.735		0.105		0.070		0.060		0.053	

* TALH, titanium(IV) bis(ammonium lactato) dihydroxide.

3. Results and Discussion

In this work, titanium(IV) bis(ammonium lactato) dihydroxide (TALH) and $\text{ZrOCl}_2 \cdot 8\text{H}_2\text{O}$ were deliberately selected to avoid dangerous (TiCl_4 and ZrCl_4) or moisture-sensitive (Ti- and Zr-alkoxides) chemicals that would complicate the synthesis procedure. Additionally, these water-soluble precursors enabled the formation of a homogeneous solution of $\text{Ti}^{4+}_{\text{aq}}$ and $\text{Zr}^{4+}_{\text{aq}}$ and their uniform precipitation with the addition of KOH, which in the further hydrothermal step ensured a more even dissolution of both precipitates ($\text{ZrO}_2 \cdot n\text{H}_2\text{O}$ and $\text{TiO}_2 \cdot n\text{H}_2\text{O}$) and consequently enabled better control of the Zr:Ti ratio in the formed PZT perovskite phase. Similar to other ABO_3 -type perovskites [13,15,16,18,22] formation of PZT under hydrothermal conditions requires an alkaline pH in which dissolved $\text{Ti}(\text{OH})_6^{2-}$ and $\text{Zr}(\text{OH})_6^{2-}$ react with dissolved Pb^{2+} and form perovskite PZT under supersaturation. The existence of $\text{Ti}(\text{OH})_6^{2-}$ and $\text{Zr}(\text{OH})_6^{2-}$ species at an alkaline pH were predicted according to the “charge-pH” diagram reported by Livage et al. [23]. In an analogy with the equation for the formation of ABO_3 perovskites under hydrothermal conditions [15,17], the PZT crystallization can be expressed by Equation (1):



Considering that the base (KOH) was involved in the formation of above-mentioned Zr- and Ti-aqueous species and the type of lead-containing species depended on the pH [24], the ratio of KOH to Pb, Zr, and Ti was a relevant parameter, not just the molarity of the KOH. For this reason, the alkaline conditions in this work are demonstrated (discussed) as the KOH:Pb ratio. When knowing the relation between the added amounts of Pb with respect to Zr and Ti, the KOH content can at any point also be expressed as the KOH:Zr or KOH:Ti ratio. We confirmed in the continuation that the ratio between the KOH and perovskite ions was important in controlling the size of the PZT crystallites and not

the absolute concentration of KOH. Xu et al. [8] observed a great variation in the size of PZT crystallites (from 4 nm nanoparticles to several-micrometer-sized cubes) with the change in KOH concentration from 4 mol/L to 1 mol/L, respectively. Inspired by this work, we decided to examine in greater detail the role of alkaline conditions in controlling the morphology of PZT particles. In particular, we focused on the conditions that could enable formation of sub-100 nm PZT crystallites, which might serve as the model system for experimental investigations of theoretically predicted configurations of the polarization field (Hopfions, vortex) in confined ferroelectrics.

3.1. Formation of the PZT with the Target Zr/Ti = 60/40 (PZT06) through One-Step Precipitation Approach

Based on the work of Xu et al. [8], PZT nanoparticles are expected to form at high KOH concentrations. For this reason, our research began with large base contents (KOH:Pb = 40:1, 30:1, and 20:1 (Table 1)) in which the initially added KOH was expected to be high enough for the precipitation of the precursors and also provided an alkaline pH for formation of the PZT perovskite phase under hydrothermal conditions. The SEM examination of the PZT06 samples that were synthesized at 235 °C for 12 h at KOH:Pb = 40:1 and 30:1 disclosed the formation of two types of morphologies. Both samples appeared very similar and were characterized by highly aggregated nanoparticles and micrometer-sized crystallites (Figure 1). Backscattered electron (BSE) images further indicated that the brighter micrometer-size crystallites consisted of elements with a higher atomic mass compared to those with a darker nanostructural phase. This was also confirmed by the EDS analyses, which showed that the nanoparticle aggregates were rich in Zr and K while Ti and Pb were present in smaller amounts. The attempt normalization of the EDS results to the perovskite ABO_3 composition did not support the perovskite structure in the nanoparticle aggregates (Table 2).

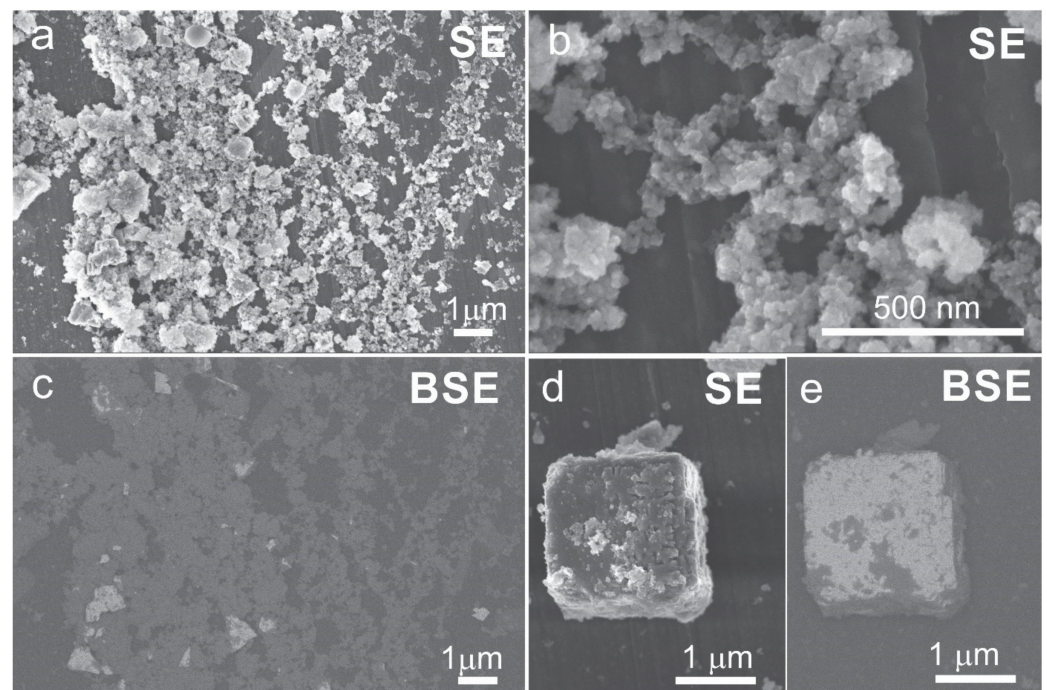


Figure 1. SEM micrographs of the PZT reaction product obtained through the one-step precipitation process and hydrothermal reaction at 235 °C (12 h) from the Zr- and Ti-precursors with initial Zr/Ti = 60/40 (PZT06) and at KOH:Pb = 30:1: (a,b,d) secondary electron (SE) images; (c,e) backscattered electron images (BSE) of the sample shown in SE images in (a) and (d), respectively.

Table 2. Summary of the main characteristics of the PZT crystallites obtained by the one-step or two-step precipitation approach at different KOH:Pb ratios.

Proposed PZT Composition (Synthesis Approach)	KOH:Pb	Typical Morphology (Average Composition as Obtained from EDS-Normalized to ABO_3 Perovskite Structure)	Average Length of Perovskite Cube Edge (Standard Deviation)
PZT06 (one-step)	30:1	Perovskite-cube-like ($Pb_{0.83}K_{0.06}Zr_{0.39}Ti_{0.68}O_3$) Zr-rich nanoparticles ($Pb_{0.14}K_{0.42}Zr_{1.12}Ti_{0.2}O_3$)	Cube-like perovskite/1–2 μm
	20:1	Perovskite cubes ($PbZr_{0.56}Ti_{0.45}O_3$)	Cubes/4 μm (1 μm)
	6:1	Perovskite cubes ($PbZr_{0.55}Ti_{0.44}O_3$)	Cubes/649 nm (80 nm)
	5:1	Perovskite cubes ($PbZr_{0.5}Ti_{0.5}O_3$)	Cubes/567 nm (72 nm)
	4:1	Perovskite cubes ($PbZr_{0.56}Ti_{0.42}O_3$)	Cubes/410 nm (48 nm)
	3:1	Perovskite dendrites ($PbZr_{0.31}Ti_{0.69}O_3$) Additional phase ($Pb_{0.69}Zr_{0.67}Ti_{0.48}O_3$)	μm -size perovskite dendrite
PZT06 (two-step)	3:1	Perovskite cubes ($PbZr_{0.55}Ti_{0.43}O_3$)	Cubes/446 nm (54 nm)
	2:1	Perovskite cubes ($PbZr_{0.52}Ti_{0.48}O_3$)	Cubes/260 nm (31 nm)
	1.7:1	Perovskite cubes ($PbZr_{0.46}Ti_{0.54}O_3$)	Cubes/172 nm (36 nm)
	1.5:1	Perovskite aggregated and cube-like particles ($Pb_{0.94}Zr_{0.46}Ti_{0.55}O_3$)	Cube-like/182 nm (48 nm)
PZT07 (two-step)	3:01	Perovskite cubes ($PbZr_{0.58}Ti_{0.41}O_3$)	Cubes/613 nm (132 nm)
	2:01	Perovskite cubes ($PbZr_{0.53}Ti_{0.47}O_3$)	Cubes/301 nm (61 nm)
	1.7:1	Perovskite cubes ($PbZr_{0.51}Ti_{0.49}O_3$)	Cube-like/241 nm (46 nm)
	1.5:1	Perovskite (aggregated) cubes ($PbZr_{0.47}Ti_{0.53}O_3$)	Cube-like/185 nm (33 nm)
PZT08 (two-step)	3:01	Perovskite cubes ($PbZr_{0.59}Ti_{0.4}O_3$)	Cubes/849 nm (117 nm)
	2:01	Perovskite cubes ($PbZr_{0.5}Ti_{0.5}O_3$)	Cube-like/355 nm (67 nm)
	1.7:1	Perovskite cubes ($PbZr_{0.52}Ti_{0.46}O_3$)	Cube-like/350 nm (75 nm)
	1.5:1	Perovskite dendrites ($Pb_{0.94}Zr_{0.31}Ti_{0.72}O_3$)	Dendrites (several μm)

On the contrary, the micrometer-sized crystallites were richer in Pb and Ti and their normalized EDS composition on average shows a good agreement with the perovskite structure. We believe that some deviation from the ideal perovskite composition was the consequence of the entanglement of both phases at several places (Figure 1d,e). In accordance with the accumulation of Zr in the nanoparticle aggregates, the Zr/Ti ratio in the micrometer-sized crystallites was smaller (39/68) than the target ratio of Zr/Ti = 60/40. The XRD patterns of both PZT06 samples (OH:Pb = 40:1 and 30:1) were identical and showed the formation of the tetragonal PZT phase, which could be indexed according to the $P4mm$ space group (ICDD PDF reference code: 04-014-6916) (Figure 2). We are confident that the tetragonal XRD reflections resulted from the micrometer-sized PZT crystallites and not from nanoparticle aggregates because the composition of the latter did not correspond to the perovskite phase. Considering that apart from the XRD diffraction lines belonging to the perovskite phase, there were no other reflections, we assumed that the Zr-rich nanoparticles were most probably amorphous or nanocrystalline with very broad and low-intensity reflections that could not be discerned from the XRD pattern. The formation of the tetragonal structure of the Ti-richer PZT phase was also in accordance with the reported PZT phase diagram [1,25]. In view of the alkaline conditions, the studied PZT06 with a KOH:Pb ratio of 40:1 corresponded to similar concentrations ratios of PZTOH (0.1 mol/L) and KOH (4 mol/L) in the research of Xu et al. [8], who reported the formation of 4 nm tetragonal PZT nanoparticles. Due to disagreement of our observations with this previous report, we focused in the next step on formation of PZT at lower KOH contents. Zr- and K-rich nanoparticle aggregates nearly disappeared at KOH:Pb = 20:1, where a few large micrometer-sized cube-like crystallites became the predominant morphology. Many of these large PZT cubes were intergrown together whereby the typical cube consisted of densely packed smaller crystallites with a size of a few 100 nm (Figures 3a and S1). According to the EDS analysis, Ti and Zr ions were incorporated in these perovskite crystallites in a ratio that was very close to the target Zr/Ti = 60/40 ratio (Table 2). In

line with the average Zr/Ti > 50/50, the rhombohedral phase with S.G. R3c (ICDD PDF: 01-078-4666) was in addition to the tetragonal phase observed in the XRD pattern of PZT06 obtained at KOH:Pb = 20:1. The dominance of the rhombohedral over the tetragonal PZT phase became the characteristic of the PZT06 samples prepared at a KOH:Pb of 6:1, 5:1, and 4:1. Apart from the rhombohedral and tetragonal phases, a monoclinic phase also could be present at PZT compositions close to MPB [26,27]. However, for clear and accurate distinction between the phases, synchrotron powder XRD measurements are required [27]. The EDS analysis revealed that all of them on average contained Zr/Ti \geq 50/50 and therefore their crystal structures were consistent with the reported phase diagram [1,25]. Good matching of the experimentally determined and target composition suggested that no secondary phase was formed. This was also confirmed by BSE microscopy (Figure 3d). The typical morphologies of these three PZT06 samples (KOH:Pb \Rightarrow 6:1, 5:1, and 4:1) were well-separated cubes, the size of which decreased from 650 nm to 410 nm for the PZT06 prepared at KOH:Pb = 6:1 and KOH:Pb = 4:1, respectively (Figures 3 and 4; Table 2). Some of the cube facets were flat, but the presence of small and rather shallow holes in the middle of the facets were also quite common (Figure 3c). Similar to the large, several-micrometer-large cubes (PZT06 \Rightarrow KOH:Pb = 20:1), some of these submicrometer-sized cubes appeared to consist of smaller intergrown particles. The particle morphology always reflected the mechanism of growth. Formation of the PZT structures under the studied hydrothermal conditions certainly occurred through the dissolution and precipitation process. However, more detailed studies are needed to elucidate whether the growth involved the template (Pb_3O_4), as proposed for the hydrothermal formation of PbTiO_3 platelets [28]; or oriented attachment [29], which is also often present in the growing of polar structures [16,30], as also was the case of PZT. According to the observed trend of a decrease in the PZT cubes with a decrease in the KOH:Pb ratio, further lowering of the size of the PZT particles might presumably be achieved by a further decrease in the KOH:Pb ratio (KOH:Pb < 4). Nevertheless, considering that OH^- ions are a prerequisite for the precipitation of lead hydroxide ($\text{PbO}\cdot\text{H}_2\text{O}$), hydrous zirconia ($\text{ZrO}_2\cdot n\text{H}_2\text{O}$), and hydrous titania ($\text{TiO}_2\cdot n\text{H}_2\text{O}$), as well as in the formation of $\text{Ti}(\text{OH})_6^{2-}$ and $\text{Zr}(\text{OH})_6^{2-}$ species under hydrothermal conditions, there were several doubts regarding whether the PZT perovskite could still form at KOH:Pb < 4 when the synthesis is performed using the one-step precipitation approach. The assumption was verified for the PZT06 at KOH:Pb = 3. The SEM examination revealed a drastic change in the morphology (Figure 3e,f). Instead of cubes, much larger dendrite-like crystallites and some other irregular morphologies appeared. The length of a typical dendrite was around 1–2 μm and consisted of several intergrown crystallites (Figure S2). BSE microscopy together with an EDS analysis confirmed that the dendrite-like structures exhibited a PZT perovskite composition with Zr/Ti = 31/69 while the additional phase contained more Zr and less Pb and Ti (Table 2). In line with the titanium-richer PZT perovskite phase, this predominantly exhibited a tetragonal crystal structure, as was evident in the XRD pattern, in which some extra diffraction lines were also present at around $35^\circ 2\theta$; these reflections could not be indexed by any known phase (Figure 2, curve f). Based on the above results, we inferred that in this low base concentration range, the incorporation of Zr into the perovskite structure required a higher pH than that of the Ti. Hence, the modification of the synthesis procedure was needed to prepare sub-100 nm PZT particles with the targeted $x = 0.6$ composition.

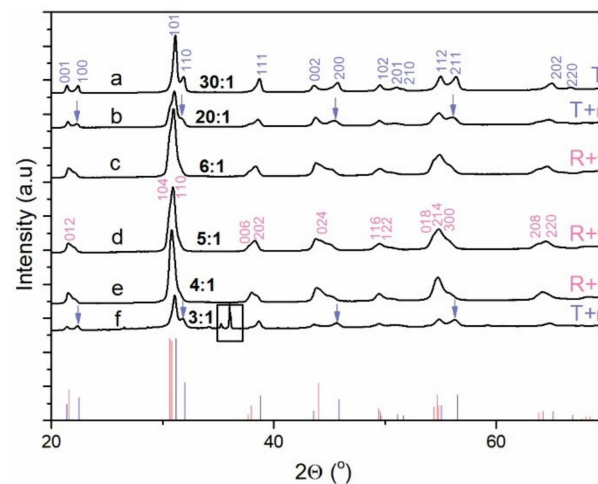


Figure 2. Powder XRD pattern of the PZT reaction product obtained through the one-step precipitation process and hydrothermal reaction at 235 °C (12 h) from the Zr- and Ti-precursors with the initial Zr/Ti = 60/40 (PZT06) and at (a) KOH:Pb = 30:1, (b) KOH:Pb = 20:1, (c) KOH:Pb = 6:1, (d) KOH:Pb = 5:1, (e) KOH:Pb = 4:1, and (f) KOH:Pb = 3:1. The main diffraction lines of rhombohedral (R) and tetragonal (T) phases were indexed according to ICDD PDF reference code 01-078-4666 and ICDD PDF reference code 04-014-6916, respectively. The prevailing phase is denoted by a larger font. The square designates the diffractions belonging to an unknown phase in the PZT06 sample, obtained at KOH:Pb = 3:1. The blue arrows indicate the occurrence of some characteristic diffractions of the tetragonal phase.

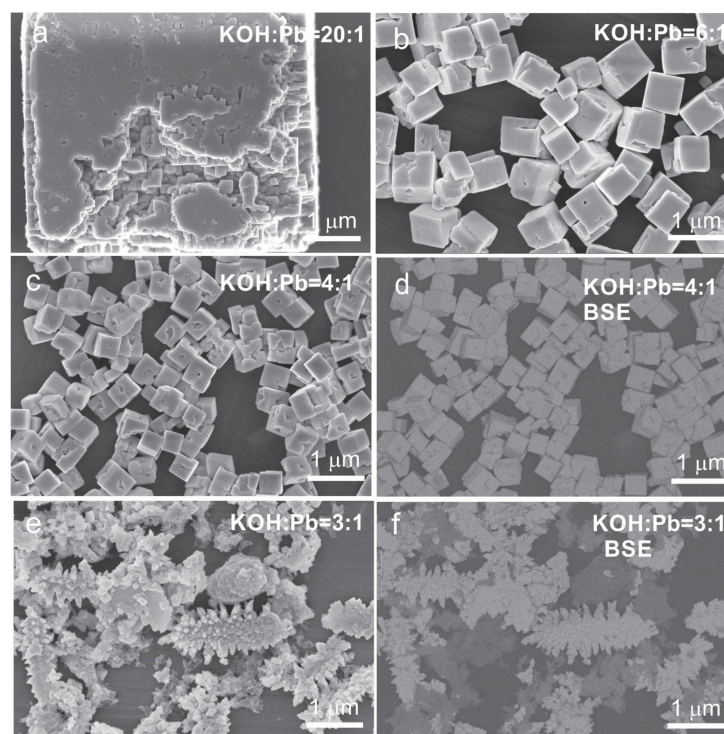


Figure 3. SEM micrographs (a–f) of the PZT06 reaction product obtained through one-step precipitation process and hydrothermal reaction at 235 °C (12 h) at (a) KOH:Pb = 20:1, (b) KOH:Pb = 6:1, (c,d) KOH:Pb = 4:1, and (e,f) KOH:Pb = 3:1: (a–c,e) ⇒ SE images; (d) and (f) ⇒ BSE images of the samples shown in the SE images in (c) and (e), respectively.

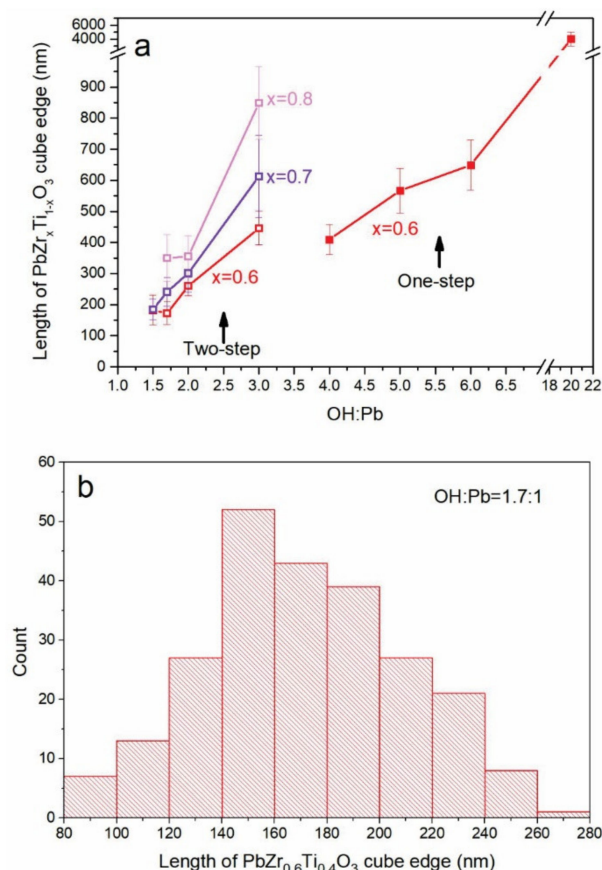


Figure 4. (a) Size of the $\text{PbZr}_x\text{Ti}_{1-x}\text{O}_3$ (PZT) cubes (length of cube edge) versus KOH:Pb ratio for the PZT synthesized through one-step (PZT06, $x = 0.6$) and two-step precipitation approaches (PZT06 ($x = 0.6$), PZT07 ($x = 0.7$), PZT08 ($x = 0.8$)). (b) Histogram of the size distribution (length of cube edge) of the PZT06 cubes obtained through two-step precipitation approach and hydrothermal synthesis at 235 °C (12 h) at KOH:Pb = 1.7:1.

3.2. Hydrothermal Formation of PZT Using Two-Step Precipitation Approach

The strategy to decrease the PZT particle size with a decrease in the KOH content (KOH:Pb ratio) was simple and appealing and consequently deserved further attention. An additional lessening of the KOH content in the hydrothermal reactor was possible when the precipitation of constituent ions was conducted in a separate step and the excessive base is washed out from the precipitate. Starting with a pH-neutral precipitate, the amount of KOH needed to provide an alkaline pH for formation of the PZT under hydrothermal conditions could be smaller and more easily controlled. In the present research, only the Zr- and Ti-precursors were precipitated in the separate step (see Table 1 in the Section 2) but not lead acetate. Specifically, due to the amphoteric nature of PbO, different soluble Pb-containing species (e.g., $\text{Pb}_6\text{O}(\text{OH})_6^{4+}$ or $\text{Pb}(\text{OH})_3^-$ [24]) might have formed with an increase in the added base in the precipitation process and therefore some loss of Pb may have occurred if a separate precipitation approach also was used for Pb^{2+} ions. The Zr^{4+} and Ti^{4+} ions were precipitated together to enable their intimate mixing in the precipitate and consequently ensure a more homogeneous dissolution ($\text{Ti}(\text{OH})_6^{2-}$ and $\text{Zr}(\text{OH})_6^{2-}$ formation) in the hydrothermal step and incorporation afterward of both ions in the PZT structure at a ratio that was close to the target composition.

3.2.1. Controlling of the PZT Particle Morphology Using Two-Step Precipitation Approach and Initial Zr/Ti = 60/40 (PZT06)

To study the variation in the PZT06 particle size as a function of the KOH concentration in the hydrothermal reactor, the syntheses of the previously precipitated Zr-Ti system with

the initial Zr/Ti = 60/40 were performed at KOH:Pb = 3:1, 2:1, 1.7:1, and 1.5:1. In these conditions, similar to those in the one-step precipitation process, the PZT particles typically adopted a cube-like shape (Figure 5). In line with the already-observed decrease in the particle size with the lowering of the KOH content, in the two-step process, the average length of the cube edge also decreased in the synthesis performed at $3 \geq \text{KOH:Pb} \geq 1.7$. For example, when the KOH:Pb ratio was changed from 3:1 to 1.7:1, the average PZT particle size decreased from approx. 450 nm to 172 nm (Figure 5a–c; Table 2). The conditions of KOH:Pb = 1.7:1 enabled the formation of the smallest and most non-aggregated PZT particles. Based on a quite broad particle size distribution, the size of a small fraction of the particles approached 100 nm; however, the desired sub-100 nm particles were very rare (Figures 4b and 5c). A further decrease in the KOH content (OH:Pb = 1.5:1) resulted in more aggregated particles (Figure 5d), whereby the size of the typical aggregate exceeded the size of the separated particles obtained at a bit higher KOH:Pb ratio equal to 1.7:1 (Figure 5c). The EDS analysis disclosed that the average composition ($\text{PbZr}_{0.55}\text{Ti}_{0.43}\text{O}_3$) of the PZT obtained at KOH:Pb = 3:1 showed the best agreement with the target $\text{PbZr}_{0.6}\text{Ti}_{0.4}\text{O}_3$ composition (Table 2). However, when the synthesis was performed at KOH:Pb = 2:1, the Zr amount had already slightly decreased ($\text{PbZr}_{0.52}\text{Ti}_{0.48}\text{O}_3$). Further lowering of the Zr content in the perovskite phase (Table 2) was observed at smaller KOH concentrations (KOH:Pb = 1.7:1 and 1.5:1), indicating that in this base concentration range the incorporation of the zirconium into the PZT perovskite phase required higher base concentrations than titanium. The crystal structural analysis revealed that rhombohedral phase was the prevailing phase for PZT obtained at $3 \geq \text{KOH:Pb} \geq 1.7$ while the tetragonal phase began to appear at KOH:Pb = 1.5:1 (Figure 6). The latter agreed with the higher Ti content with respect to Zr in the perovskite phase (Table 2) as well as with the reported PZT phase diagram [1,25].

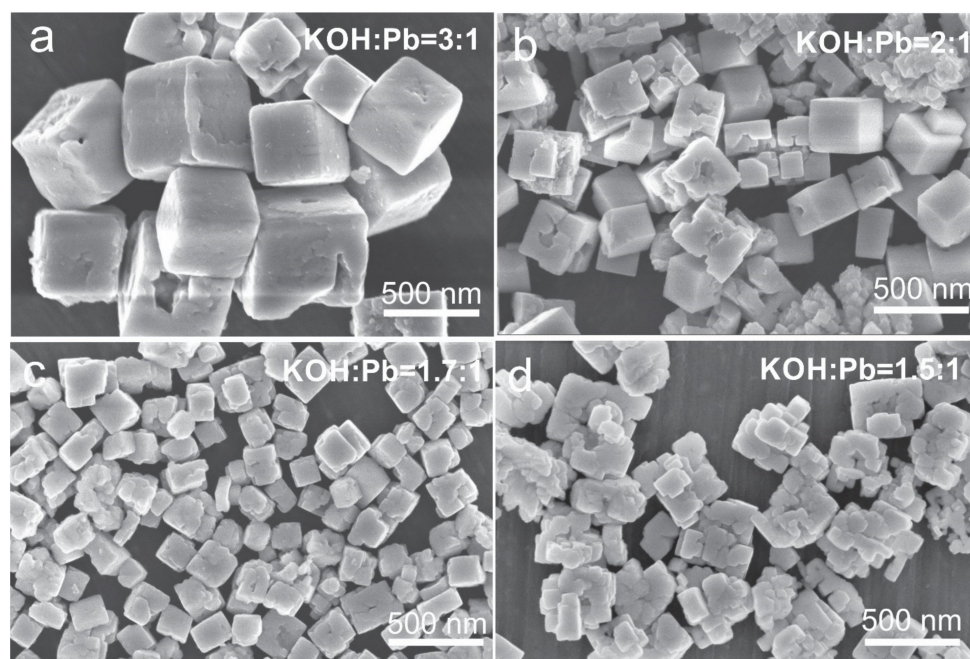


Figure 5. SEM micrographs (SE images) of the PZT06 reaction product obtained through two-step precipitation process and hydrothermal reaction at 235 °C (12 h) and at (a) KOH:Pb = 3:1, (b) KOH:Pb = 2:1, (c) KOH:Pb = 1.7:1, and (d) KOH:Pb = 1.5:1. The optimal morphology (well-separated small PZT particles (80–280 nm (Figure 4)) are shown in (c) (KOH:Pb = 1.7:1).

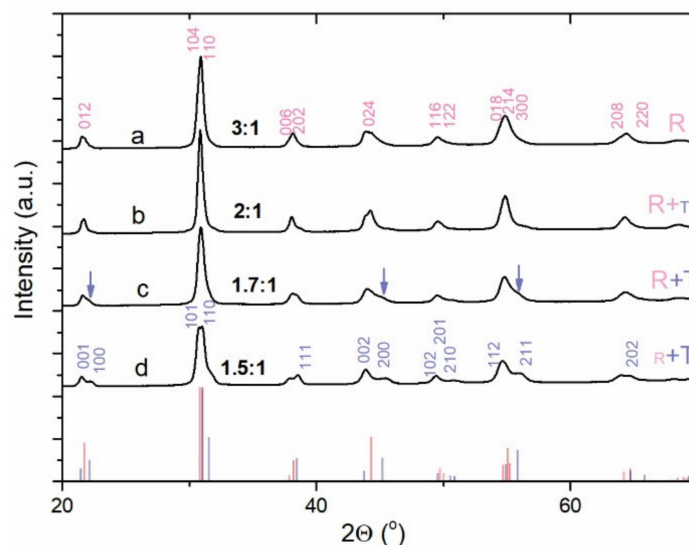


Figure 6. Powder XRD pattern of the PZT06 reaction product obtained through two-step precipitation process and hydrothermal reaction at 235 °C (12 h) and at (a) KOH:Pb = 3:1, (b) KOH:Pb = 2:1, (c) KOH:Pb = 1.7:1, and (d) KOH:Pb = 1.5:1. The main diffraction lines of rhombohedral (R) and tetragonal (T) phase were indexed according to ICDD PDF reference code 01-070-4262 (S.G.: P4mm) and ICDD PDF reference code 04-012-9961 (S.G.: R3c), respectively. The prevailing phase is denoted by a larger letter. The blue arrows indicate the occurrence of some characteristic diffractions of the tetragonal phase.

Understanding of the chemistry of the hydrothermal transformation implied that concentration of the base (KOH) with respect to the metal ions constituting the PZT was important in governing the transformation process and consequently determined the morphology of the final PZT particles. Without knowing these concentration relations, the role of KOH concentration in the PZT formation could not be well interpreted. To confirm this empirical prediction, two synthesis experiments with a double concentration of Pb, Zr, and Ti with respect to those presented in Table 1 (PZT06 (two-step), KOH:Pb = 3:1) were performed. In the first synthesis trial, the concentration of KOH was also two times higher, leading to KOH:Pb = 3:1; while in the next synthesis the absolute concentration of KOH was the same as for the usual synthesis (0.105 mol/L), resulting in KOH:Pb = 1.5:1. A comparison of the morphologies (Figure S3) revealed that when KOH:Pb = 3:1, PZT cubes with a similar size formed irrespective of the double difference in the concentrations of the Pb, Zr, and Ti precursors. When the KOH concentration remained the same while the contents of Pb, Zr, and Ti were doubled, the final PZT morphology again resembled that of the usual experiment with the same KOH:Pb ratio equal to 1.5:1 and not the morphology obtained in the usual experiment with the same absolute KOH concentration. The results undoubtedly highlighted the importance of the consideration of the concentration relations between the base and perovskite ions in the designing of the PZT perovskite particles.

3.2.2. Controlling of the PZT Particle Morphology Using Two-Step Precipitation Approach and Initial Zr/Ti = 70/30 (PZT07) and Zr/Ti = 80/20 (PZT08)

In view of larger PZT particle growth at higher KOH concentrations, the increment in the KOH:Pb ratio was not the right strategy to achieve the target Zr/Ti = 60/40 composition and fulfill the requirement of small sub-100 nm PZT particles. For this reason, we attempted to enhance the incorporation of zirconium in the perovskite phase by increasing the Zr content in the precursor solution. For a better understanding of the correlations between the concentrations, morphology, crystal structure, and final compositions of the formed perovskite phase, the syntheses of the PZT particles began with the precursor solutions with higher initial Zr/Ti = 70/30 (PZT07) and Zr/Ti = 80/20 (PZT08) and were performed in hydrothermal conditions with controlled KOH contents in the range of $1.5 \leq \text{KOH:Pb} \leq 3$.

The formation of the cubes, the size of which decreased with KOH:Pb but increased with the initial Zr:Ti ratio (Figure 4) and enhanced aggregation, particularly at KOH:Pb = 1.5 (Figures 7 and 8), all clearly showed that the approach of using higher initial Zr:Ti ratios was far from beneficial in the preparation of sub-100 nm PZT particles with the target Zr/Ti = 60/40. Nevertheless, the understanding of the structural and compositional development could still provide useful information that improved the comprehension of the hydrothermal PZT formation. As was evident in the EDS analysis, the Zr content in the PZT was the highest (Zr/Ti = 60/40) at KOH:Pb = 3:1 and was the same for both initial Zr/Ti ratios of 70/30 and 80/20 (Table 2). These results implied that at KOH:Pb = 3, the amount of incorporated Zr could not be enhanced by the increase in the Zr/Ti ratio in the precursor solution. Similarly, as observed for the initial Zr/Ti = 60/40, the Zr/Ti ratio in the formed perovskite phase decreased with a decrease in the KOH concentration despite higher initial Zr/Ti ratios of 70/30 and 80/20 (Table 2). The lowest Zr content was observed in the perovskite dendrites that formed from the precursors at the initial Zr/Ti = 80/20 and KOH:Pb = 1.5:1 (Figure 8d). Similar to the initial Zr/Ti = 60/40, the crystal structure was rhombohedral at OH:Pb = 3:1 and the tetragonal phase began to appear at lower KOH contents (Figures S4 and S5).

The above findings again confirmed that under these hydrothermal conditions the incorporation of zirconium into the perovskite lattice compared to titanium required a higher base concentration, which inversely led to larger particle sizes. In light of such conclusions, the formation of sub-100 nm PZT particles at Zr/Ti = 60/40 seemed to be somehow elusive in the present experimental conditions. Nevertheless, PZT particles with a size close to 100 nm and a composition of Zr/Ti = 46/54 that formed at OH:Pb = 1.7:1 from the initial Zr/Ti = 60/40 showed that with the appropriate modification of the experimental conditions, the target morphology and composition of the PZT are achievable.

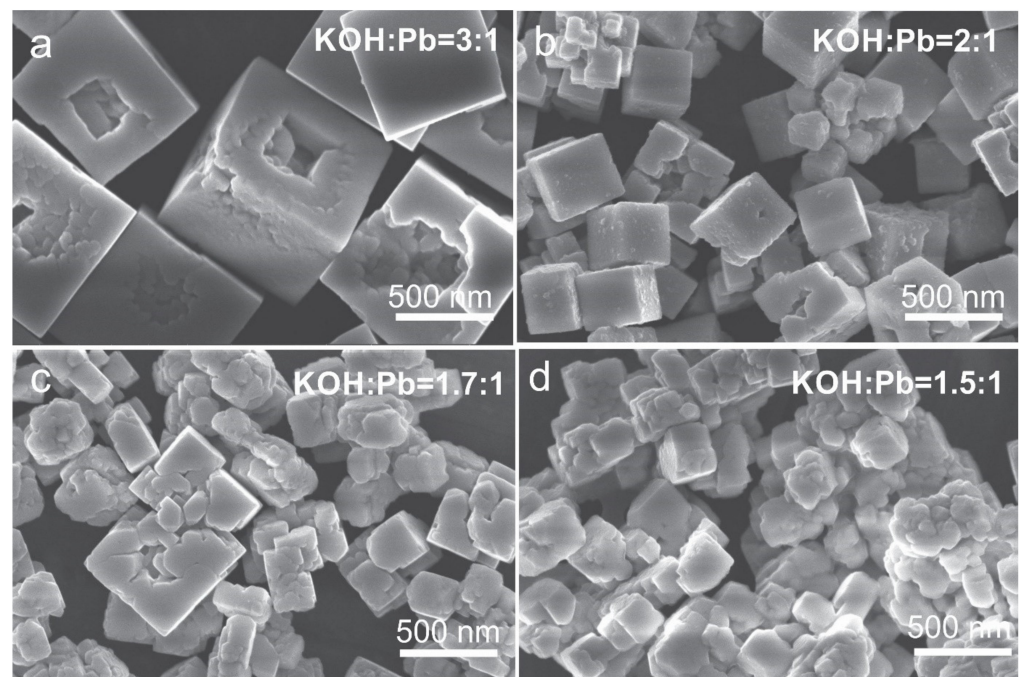


Figure 7. SEM micrographs (SE images) of the PZT07 reaction product obtained through two-step precipitation process and hydrothermal reaction at 235 °C (12 h) and at (a) KOH:Pb = 3:1, (b) KOH:Pb = 2:1, (c) KOH:Pb = 1.7:1, and (d) KOH:Pb = 1.5:1.

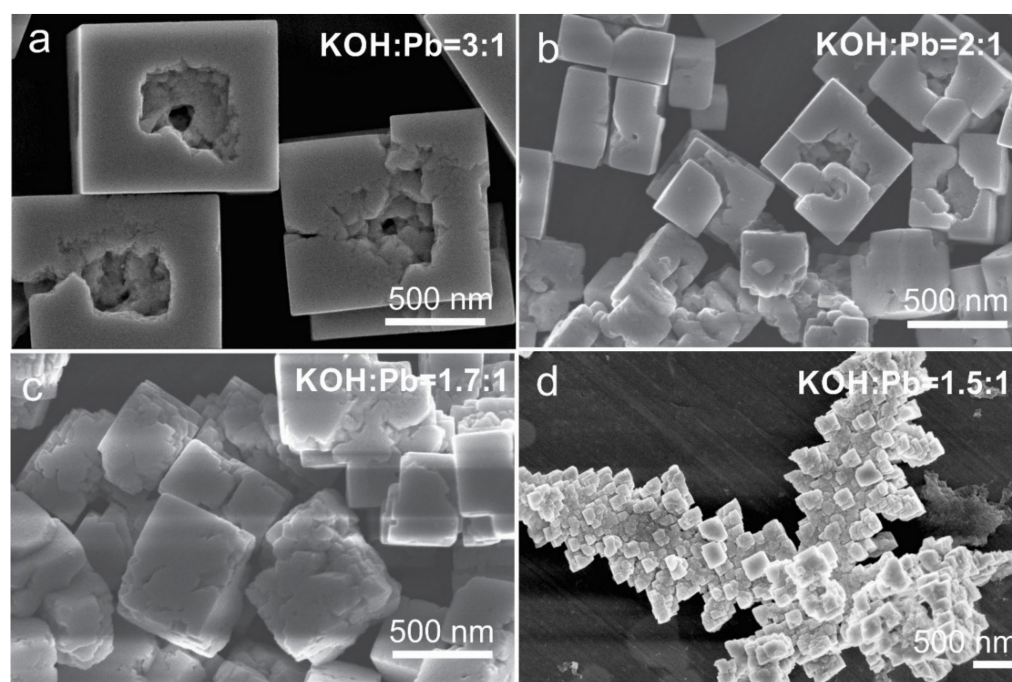


Figure 8. SEM micrographs (SE images) of the PZT08 reaction product obtained through two-step precipitation process and hydrothermal reaction at 235 °C (12 h) and at (a) KOH:Pb = 3:1, (b) KOH:Pb = 2:1, (c) KOH:Pb = 1.7:1, and (d) KOH:Pb = 1.5:1.

4. Conclusions

The formation of PZT from water-soluble Zr-, Ti- and Pb-precursors in different alkaline (KOH) hydrothermal conditions was investigated to identify the key concentration correlations that governed the PZT particle morphology, crystal structure, and composition. We found that PZT crystallized in the target composition (Zr/Ti = 60/40) and rhombohedral structure in a limited range of concentration ratios between KOH and Pb ions. In the one-step precipitation approach, zirconium did not incorporate entirely in the PZT phase at KOH:Pb > 20 and at KOH:Pb ≤ 3. In the concentration range of 20 > KOH:Pb ≥ 4, the PZT perovskite particles adopted a cube shape, were well separated, and became smaller at lower KOH:Pb ratios. The formation of PZT at lower KOH:Pb ratios and consequently smaller PZT particle sizes was achieved via preparation of a pH-neutral Zr-Ti precipitate before the hydrothermal reaction at 235 °C for 12 h (two-step precipitation approach). Using this strategy, the PZT particle size was decreased to less than 200 nm and the particles remained well separated for KOH:Pb = 1.7; the average Zr/Ti ratio was 46/54. Diminished Zr incorporation with a decrease in the KOH:Pb, which was particularly notable at KOH:Pb ≤ 1.7, indicated that Zr ions required a higher base concentration for incorporation into the PZT perovskite structure than Ti ions did. The PZT particles exhibited a rhombohedral crystal structure at a Zr/Ti around 60/40; however, with a decrease to Zr/Ti < 50/50, a tetragonal phase also appeared. Unravelling of the above-described relationships will pave the way to further design of PZT ferroelectric (nano)particles in line with the needs of fundamental studies or practical application.

Supplementary Materials: The following supporting information can be downloaded at: <https://www.mdpi.com/article/10.3390/cryst12111514/s1>, Figure S1: SEM micrograph (SE image) of the PZT06 reaction product obtained through one-step precipitation process and hydrothermal reaction at 235 °C (12 h) at KOH:Pb = 20:1; Figure S2: SEM micrographs (a,b) of the PZT06 reaction product obtained through one-step precipitation process and hydrothermal reaction at 235 °C (12 h) at KOH:Pb = 3:1: (a) ⇒ SE image, b ⇒ BSE image; Figure S3: SEM micrographs of the PZT06 reaction product obtained through two-step precipitation process and hydrothermal reaction at 235 °C (12 h) (a,b) using the concentrations of Pb-, Zr- and Ti-precursors as shown in Table 1

($C_{\text{TALH}} = 0.0112$ mol/L, $C_{\text{ZrOCl}_2} = 0.0168$ mol/L, and $c_{\text{Pb}(\text{CH}_3\text{COO})_2} = 0.035$ mol/L) and (c,d) two-times larger concentrations of Pb-, Zr- and Ti-precursors ($C_{\text{TALH}} = 0.0224$ mol/L, $C_{\text{ZrOCl}_2} = 0.0336$ mol/L, and $c_{\text{Pb}(\text{CH}_3\text{COO})_2} = 0.07$ mol/L). The concentrations of KOH were doubled in (c), resulting in KOH:Pb = 3:1, but in (d) remained the same as for the normal Pb- Zr-, and Ti-concentration experiments (0.1 mol/l), resulting in KOH:Pb = 1.5:1; Figure S4: Powder XRD pattern of the PZT07 reaction product obtained through two-step precipitation process and hydrothermal reaction at 235 °C (12 h) and at (a) KOH:Pb = 3:1, (b) KOH:Pb = 1.7:1, and (c) KOH:Pb = 1.5:1. The main diffraction lines of the rhombohedral (R) and tetragonal (T) phase were indexed according to ICDD PDF reference code 04-016-9524 (S.G.: R3c) and ICDD PDF reference code 01-070-4262 (S.G.: P4mm), respectively. The prevailing phase is denoted by a larger letter. The blue arrows indicate the occurrence of some characteristic diffractions of the tetragonal phase; Figure S5: Powder XRD pattern of the PZT08 reaction product obtained through two-step precipitation process and hydrothermal reaction at 235 °C (12 h) and at (a) OH:Pb = 3:1, (b) KOH:Pb = 1.7:1, and (c) KOH:Pb = 1.5:1. The main diffraction lines of the rhombohedral (R) and tetragonal (T) phase were indexed according to ICDD PDF reference code 01-078-4666 (S.G.: R3c) and ICDD PDF reference code 04-017-5715 (S.G.: P4mm), respectively. The prevailing phase is denoted by a larger letter. The blue arrows indicate the occurrence of some characteristic diffractions of the tetragonal phase.

Author Contributions: Conceptualization of the target composition and morphology, Z.K. and M.S.; conceptualization of the synthesis approach and methodology, M.M.K.; investigation, M.M.K.; writing—original draft preparation, M.M.K.; writing—review and editing, M.M.K. and M.S. All authors have read and agreed to the submitted version of the manuscript.

Funding: This research was funded by the Slovenian Research Agency (research program no. P2-0091) and the Ministry of Higher Education, Science and Technology, M-era.Net, under project SunToChem (no. 6081; contract no. C3330-19-252011).

Acknowledgments: The authors are grateful to Mihael Turkovic for his help in the extensive synthesis work.

Conflicts of Interest: The authors declare no conflict of interest.

References

1. Noheda, B.; Cox, D.E.; Shirane, G.; Guo, R.; Jones, B.; Cross, L.E. Stability of the monoclinic phase in the ferroelectric perovskite $\text{PbZr}_{1-x}\text{Ti}_x\text{O}_3$. *Phys. Rev. B* **2000**, *63*, 014103. [[CrossRef](#)]
2. Dong, N.; Zhu, K.; Qiu, J.; Liu, J. Sol-solvothermal synthesis and characterization of fine lead zirconate titanate particles. *J. Mater. Sci. Mater. Electron.* **2013**, *24*, 2264–2270. [[CrossRef](#)]
3. Meng, Q.; Zhu, K.; Pang, X.; Qiu, J.; Shao, B.; Ji, H. Sol-hydrothermal synthesis and characterization of lead zirconate titanate fine particles. *Adv. Powder Technol.* **2013**, *24*, 212–217. [[CrossRef](#)]
4. Huang, H.L.; Cao, G.Z.; Shen, I.Y. Hydrothermal synthesis of lead zirconate titanate (PZT or $\text{Pb}(\text{Zr}_{0.52}\text{Ti}_{0.48})\text{O}_3$) nano-particles using controlled ramping and cooling rates. *Sens. Actuators A Phys.* **2014**, *214*, 111–119. [[CrossRef](#)]
5. Malic, B.; Arcon, I.; Kodre, A.; Kosec, M. Homogeneity of $\text{Pb}(\text{Zr,Ti})\text{O}_3$ thin films by chemical solution deposition: Extended x-ray absorption fine structure spectroscopy study of zirconium local environment. *J. Appl. Phys.* **2006**, *100*, 051612. [[CrossRef](#)]
6. Wu, A.; Vilarinho, P.M.; Miranda Salvado, I.M.; Baptista, J.L. Sol-gel preparation of lead zirconate titanate powders and ceramics: Effect of alkoxide stabilizers and lead precursors. *J. Am. Ceram. Soc.* **2000**, *83*, 1379–1385. [[CrossRef](#)]
7. Lazar, I.; Majchrowski, A.; Soszyński, A.; Roleder, K. Phase Transitions and Local Polarity above TC in a $\text{PbZr}_{0.87}\text{Ti}_{0.13}\text{O}_3$ Single Crystal. *Crystals* **2020**, *10*, 286. [[CrossRef](#)]
8. Xu, G.; Jiang, W.; Qian, M.; Chen, X.; Li, Z.; Han, G. Hydrothermal synthesis of lead zirconate titanate nearly free-standing nanoparticles in the size regime of about 4 nm. *Cryst. Growth Des.* **2009**, *9*, 13–16. [[CrossRef](#)]
9. Chen, J.X.; Li, J.W.; Cheng, C.C.; Chiu, C.W. Piezoelectric Property Enhancement of PZT/Poly(vinylidene fluoride-co-trifluoroethylene) Hybrid Films for Flexible Piezoelectric Energy Harvesters. *ACS Omega* **2022**, *7*, 793–803. [[CrossRef](#)]
10. Luk'yanchuk, I.; Tikhonov, Y.; Razumnaya, A.; Vinokur, V.M. Hopfions emerge in ferroelectrics. *Nat. Commun.* **2020**, *11*, 1–7. [[CrossRef](#)]
11. Panda, P.K.; Sahoo, B. PZT to lead free piezo ceramics: A review. *Ferroelectrics* **2015**, *474*, 128–143. [[CrossRef](#)]
12. Koruza, J.; Bell, A.J.; Frömling, T.; Webber, K.G.; Wang, K.; Rödel, J. Requirements for the transfer of lead-free piezoceramics into application. *J. Mater.* **2018**, *4*, 13–26. [[CrossRef](#)]
13. Maček Kržmanc, M.; Klement, D.; Jančar, B.; Suvorov, D. Hydrothermal conditions for the formation of tetragonal BaTiO_3 particles from potassium titanate and barium salt. *Ceram. Int.* **2015**, *41*, 15128–15137. [[CrossRef](#)]
14. Čontala, A.; Kržmanc, M.M.; Suvorov, D. Plate-like $\text{Bi}_4\text{Ti}_3\text{O}_{12}$ particles and their topochemical conversion to SrTiO_3 under hydrothermal conditions. *Acta Chim. Slov.* **2018**, *65*, 630–637. [[CrossRef](#)] [[PubMed](#)]

15. Maček Kržmanc, M.; Daneu, N.; Čontala, A.; Santra, S.; Kamal, K.M.; Likozar, B.; Spreitzer, M. SrTiO₃/Bi₄Ti₃O₁₂ Nanoheterostructural Platelets Synthesized by Topotactic Epitaxy as Effective Noble-Metal-Free Photocatalysts for pH-Neutral Hydrogen Evolution. *ACS Appl. Mater. Interfaces* **2021**, *13*, 370–381. [[CrossRef](#)]
16. Maček Kržmanc, M.; Bračko, I.; Budič, B.; Suvorov, D. The morphology control of BaTiO₃ particles synthesized in water and a water/ethanol solvent. *J. Am. Ceram. Soc.* **2013**, *96*, 3401–3409. [[CrossRef](#)]
17. Kalyani, V.; Vasile, B.S.; Ianculescu, A.; Testino, A.; Carino, A.; Buscaglia, M.T.; Buscaglia, V.; Nanni, P. Hydrothermal Synthesis of SrTiO₃: Role of Interfaces. *Cryst. Growth Des.* **2015**, *15*, 5712–5725. [[CrossRef](#)]
18. Canu, G.; Buscaglia, V. Hydrothermal synthesis of strontium titanate: Thermodynamic considerations, morphology control and crystallisation mechanisms. *CrystEngComm* **2017**, *19*, 3867–3891. [[CrossRef](#)]
19. Cheng, H.; Ma, J.; Zhu, B.; Cui, Y. Reaction Mechanisms in the Formation of Lead Zirconate Titanate Solid Solutions under Hydrothermal Conditions. *J. Am. Ceram. Soc.* **1993**, *76*, 625–629. [[CrossRef](#)]
20. Traianidis, M.; Courtois, C.; Leriche, A.; Thierry, B. Hydrothermal synthesis of lead zirconium titanate (PZT) powders and their characteristics. *J. Eur. Ceram. Soc.* **1999**, *19*, 1023–1026. [[CrossRef](#)]
21. Piticescu, R.M.; Moisin, A.M.; Taloi, D.; Badilita, V.; Soare, I. Hydrothermal synthesis of ultradisperse PZT powders for polar ceramics. *J. Eur. Ceram. Soc.* **2004**, *24*, 931–935. [[CrossRef](#)]
22. Lencka, M.M.; Riman, R.E. Thermodynamic Modeling of Hydrothermal Synthesis of Ceramic Powders. *Chem. Mater.* **1993**, *5*, 61–70. [[CrossRef](#)]
23. Livage, J.; Henry, M.; Sanchez, C. Sol-gel chemistry of transition metal oxides. *Prog. Solid State Chem.* **1988**, *18*, 259–341. [[CrossRef](#)]
24. Wiberg, V.E.; Wiberg, N.; Holleman, A.F. *Inorganic Chemistry*; Academic Press: Cambridge, MA, USA, 2001.
25. Jaffe, B.; Cook, W.R.; Jaffe, H. *Piezoelectric Ceramics*, 1st ed.; Academic Press: Cambridge, MA, USA, 1971; ISBN 978-0-12-379550-2.
26. Courtois, C.; Crampon, J.; Champagne, P.; Cochrane, C.; Texier, N.; Leriche, A. STEM-X-EDS analysis of morphotropic PZT ceramics. Analysis of Zr/Ti + Zr values fluctuation depending on microstructure and synthesis route of powders. *Ceram. Int.* **2006**, *32*, 767–773. [[CrossRef](#)]
27. Noheda, B.; Gonzalo, J.A.; Cross, L.E.; Guo, R.; Park, S.-E.; Cox, D.E.; Shirane, G. Tetragonal-to-monoclinic phase transition in a ferroelectric perovskite: The structure of PbZr_{0.52}Ti_{0.48}O₃. *Phys. Rev. B* **2000**, *61*, 8687–8695. [[CrossRef](#)]
28. Chao, C.; Ren, Z.; Zhu, Y.; Xiao, Z.; Liu, Z.; Xu, G.; Mai, J.; Li, X.; Shen, G.; Han, G. Self-templated synthesis of single-crystal and single-domain ferroelectric nanoplates. *Angew. Chem. Int. Ed.* **2012**, *51*, 9283–9287. [[CrossRef](#)] [[PubMed](#)]
29. Niederberger, M.; Cölfen, H. Oriented attachment and mesocrystals: Non-classical crystallization mechanisms based on nanoparticle assembly. *Phys. Chem. Chem. Phys.* **2006**, *8*, 3271–3287. [[CrossRef](#)] [[PubMed](#)]
30. Dang, F.; Kato, K.; Imai, H.; Wada, S.; Haneda, H.; Kuwabara, M. Oriented aggregation of BaTiO₃ nanocrystals and large particles in the ultrasonic-assistant synthesis. *CrystEngComm* **2010**, *12*, 3441–3444. [[CrossRef](#)]